CHAPTER 4 ANALYTICAL TECHNIQUES

This chapter discusses the main analysing techniques used in the study of silver diffusion and the production and annealing of radiation damage in 6H-single crystalline SiC. The main techniques used in this thesis are Rutherford backscattering spectrometry (RBS), RBS combined with channelling (RBS-C) and Scanning Electron Microscopy (SEM).

4.1 RUTHERFORD BACKSCATTERING SPECTROSCOPY - CHANNELLING (RBS-C)

In discussing these techniques we start by discussing the important parameters of the RBS and RBS-C techniques in section 4.1.1, followed by the details of the RBS technique in section 4.1.2; RBC-C is considered in section 4.2 and SEM in section 4.3.

4.1.1 ACCELERATOR, SCATTERING CHAMBER AND DETECTOR SYSTEM

RBS is a technique that is based on the analysis of the energy of the backscattered charged particles (helium ions (He^+) in our case) from the particular material of interest: for example in this thesis it is single crystal-6H silicon carbide with silver either deposited or implanted. The charged particles are generated by a RF-source and accelerated to high energies by applying a large potential difference across the accelerator tube. All this is done by a Van de Graaff accelerator which uses the principles discovered many years ago [Gra31]. This accelerator generates a high voltage using a moving insulating belt that carries charge which is sprayed on at the base plate and removed at the terminal. The work reported in this thesis was performed using the Van de Graaff accelerator at the University of Pretoria. The maximum voltage of this machine is 2.7 MeV but an energy of 1.6 MeV was used in this investigation. Schematic diagrams of the accelerator and the scattering chamber are reproduced in figure 4-1 (a) and (b).

The dipole magnet in front of the Van de Graaff accelerator deflects the beam into either beam line 1 or line 2. Hence, it acts as an energy and mass separator. Beam

line 1 has a chamber that is designed to operate below room temperature while line 2 functions at room temperature. For this study line 2 was used. A combination of vertical and horizontal slits in line 2 focuses and guides the beam into the chamber. The slits also help in producing a monochromatic beam consisting of one species, i.e. helium ions. The collimator inside the chamber (figure 4-1(b)) shapes the beam into a specific size before interacting with the sample. Thus the size of the beam is determined by the collimator's size. The sample is fixed on a stainless steel sample holder connected on a three axis goniometer system which has a precision of 0.02^{o} in each of the angle settings. The secondary electrons, which falsify the measurements, are suppressed by a negative voltage of 200 V connected to a ring shaped electrode in front of the target.

During analyses the beam is kept below 15 nA to avoid heating of the sample. This is also done to avoid a pile-up effect during the process of detecting backscattered particles. Pile-up occurs when the time response of the detector system is not fast enough to separate the individual events on the detector due to the high rate of encountered events. Therefore, in such a situation two events may end up being recorded as one event, which will falsify the measurements. The hydrocarbon deposition on the sample during analyses is minimised by keeping the pressure in the chamber at 10^{-4} Pa or below during the process. This carbon deposition is due to the collision of the analysing particles/beam with the residual gases and the subsequent decomposition of the gases. This occurs along the beam line but the carbon that is deposited on the sample's surface is that produced near the sample surface. The adsorption of water and carbon dioxide inside the chamber's surface is minimised by flooding the chamber with nitrogen gas during the opening of the chamber. This also helps in increasing the initial pumping rate.

The backscattered alpha particles represented by BS in figure 4-1(b) are detected by a Si surface barrier detector operating with a reverse bias of 40 V. The output charge signal (proportional to the energy of the backscattered particles) of the detector is fed into the pre-amplifier where it is integrated into a voltage signal that is proportional to the backscattered energy. This voltage signal is then amplified by the amplifier before it is digitized by an analogue to digital converter (ADC) inside the multi-channel analyzer (MCA) and stored in the computer connected to the MCA. The output of

MCA consists of counts vs. the channel number spectrum. The yield is the number of backscattered particles at 165^{o} (for our experimental set-up) while the channel number is proportional to the backscattered energy. Using the computer, together with the RBS and RBS-C spectrum, the counts of backscattered ions as a function of channel number are monitored online and saved in the computer. The position of the sample is fixed but its orientation can be changed using the three axis goniometer with a digitized control unit that is controlled manually. Data acquisition is discussed in detail in section 5.5.

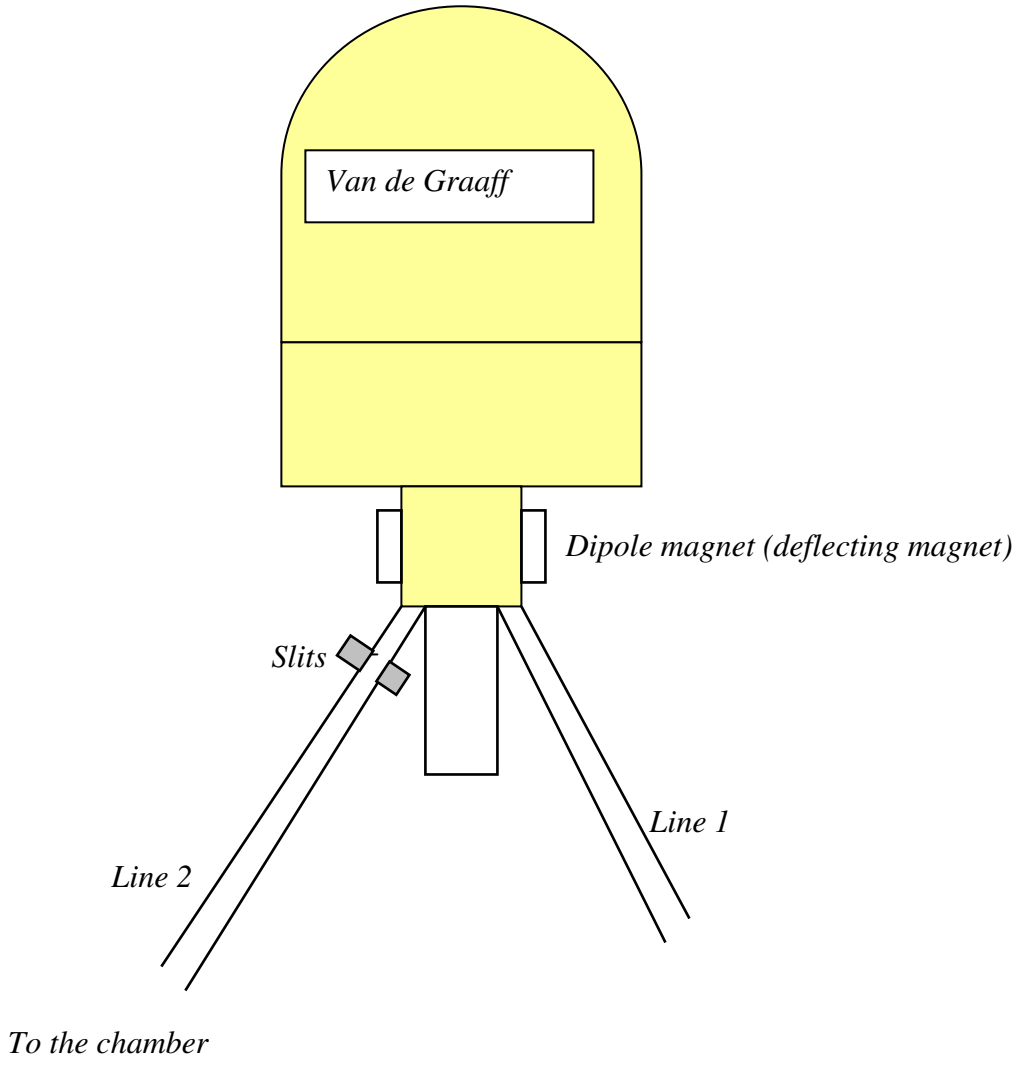

Figure 4-1 (a): A schematic diagram showing the Van de Graaff accelerator and beam lines of the University of Pretoria.

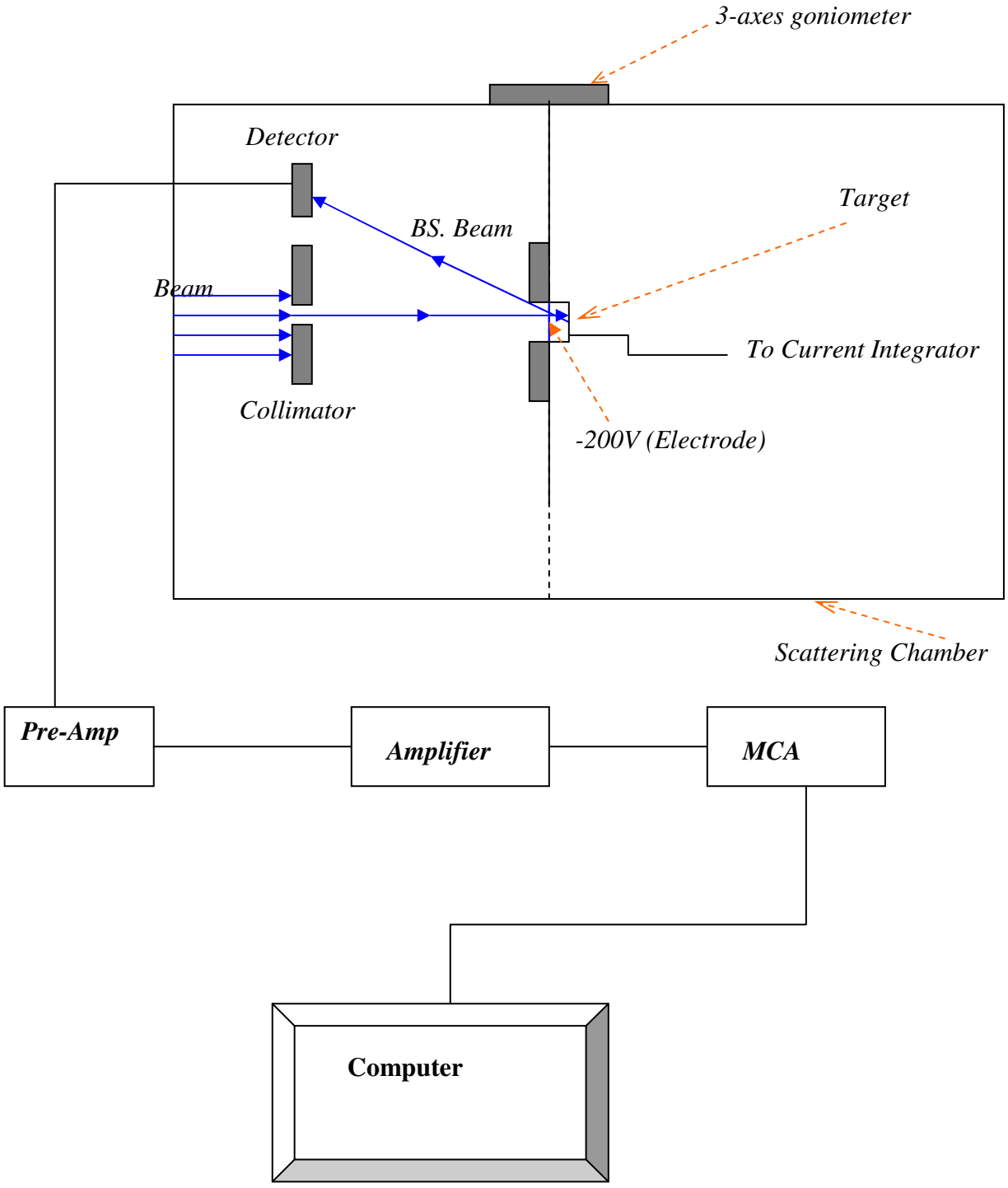

Figure 4-1(b): A schematic diagram showing the side view of the scattering chamber and detector system for the University of Pretoria's Van de Graaff accelerator.

4.1.2 DETAILS OF RUTHERFORD BACKSCATTERING SPECTROSCOPY

The non-destructive nature, simplicity, identification power, possibility of simultaneous multi element profiling and good depth resolution has caused RBS to dominate ion beam analysis in thin film science. Since this technique is based on the detection of backscattered alpha particles, the detector is placed at an angle greater than 90^{o} but less than 180^{o} with respect to the incoming beam – see Figure 4-2 for the definition of the angle. Therefore, only the backscattered alpha particles are detected. In this case the backscattered yield vs. channel number is measured. From the measured spectra the information about masses and the depth distribution of the target elements are extracted. This is only achieved if the kinematic factor, stopping power and scattering cross section of the ions are well understood. Therefore, all the above factors are discussed in this section together with some other factors that perturb the accuracy of RBS measurements.

4.1.3 KINEMATIC FACTOR

The setup of the RBS-C used in this thesis is illustrated in figure 4-2 below: In this setup the target is placed in such a way that the surface is facing the incoming α-beam and the detector is placed at the backscattered angle of 165^{o} with respect to the incoming beam (see figure 4-2). For random RBS measurements the sample is oriented 5^{o} off the channelled direction, as was discussed in section 4.2. The three angular parameters of the goniometer are digitized and not automated (see figure 4-1(b)). When the incoming beam collides with the target some of the target atoms recoil at angle ϕ (see figure 4.2) with respect to the incident beam.

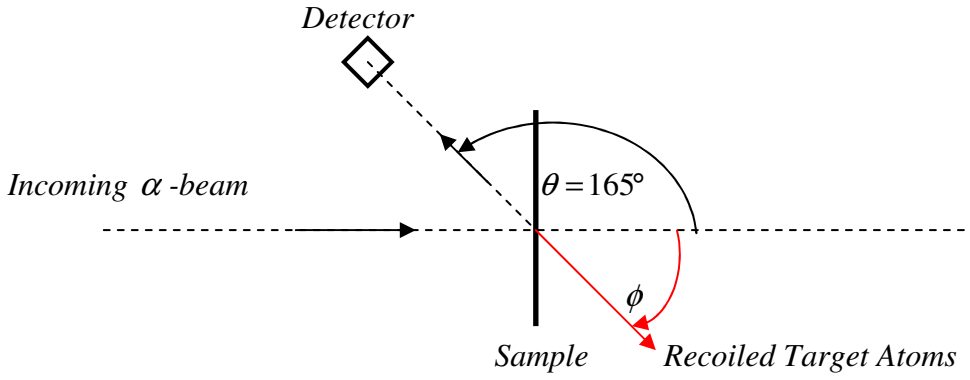

Figure 4-2: A schematic diagram showing the RBS experimental setup at the University of Pretoria.

If only elastic collisions are considered in such a setup, the energy of the backscattered α-particle (E_1) can be calculated using the conservation of energy and momentum [Chu78] [Tes95]:

$$E_1 = KE_0 = \left[\frac{M_1 \cos\theta \pm (M_2^{\,2} - M_1^{\,2}\sin^2\theta)^{1/2}}{M_1 + M_2}\right]^2 E_0 \qquad \ldots 4.1$$

where E_0 and E_1 is the energy of the incident and backscattered α-particles respectively, M_1 and M_2 are the masses of the analysing particle (α-particle) and the target atom, K is the kinematic factor (the ratio of the backscattered particle's energy to incident energy before scattering) and θ is the backscattering angle.

From equation 4.1 one can observe that E_1 can be calculated if the kinematic factor K is known. K can be calculated using M_1, M_2 and the scattering angle θ. At a fixed scattering angle the kinematic factor K depends only on the mass ratio i.e. M_1/M_2. The plus sign in equation 4 is only valid for the case where $M_1 < M_2$, while for $M_1 > M2$ there are two solutions, resulting in two kinematic factors K for backscattered α-particles at angle θ corresponding to different recoil angles ϕ [Chu78].

The RBS technique can be used to identify the sample components because the α-particles with the same incident energy and incident angle backscattered at different masses yield different energies according to equation 4.1. This difference in scattering energy for different masses influences the depth resolution, which is limited by a number of factors. These are: the energy resolution of the detector, the spread in energy of the α-particle, the solid angle of the detector, the beam size and the divergence of the accelerator beam. Good mass resolution is usually accomplished by using a projectile of higher mass but not larger than the target mass atom (because in the case where $M_1 > M_2$ the projectile will not backscatter) and measuring at a backscattering angle that is approximately 180^{o}. In this study α-particles were used to minimise the energy straggling compared to other heavy atoms such as oxygen.

4.1.4 DEPTH PROFILING

The backscattered alpha particles also have different energies because they are backscattered from different depths. For example, figure 4-3 is a schematic diagram

depicting the backscattering events at the surface and at depth x. The alpha particle that backscatters at the surface possesses energy of KE_0 while the one that backscatters at depth x has an initial energy E lower than E_0 because it loses energy before backscattering at depth x. From figure 4-3, the length of the inward path where the ion loses energy is $x/cos\theta_1$. As can be seen in figure 4-3 the ion has energy KE just after being backscattered at depth x. The ion that is backscattered at depth x continues to lose energy on its way out; with reference to figure 4-3 it is evident that the length of the outward path is $x/cos\theta_2$.

In order to calculate the energy of the alpha particle that backscatters at depth x one needs to take into consideration the fact that it loses energy both on its way in and out. The expression of the alpha particle that backscattered at depth x was derived by assuming that the energy loss (dE/dx) is constant along the inward and outward paths [Chu78] [Tes95]:

$$KE_0 - E_1 = \left[\frac{K}{\cos\theta_1} \frac{dE}{dx}(in) + \frac{1}{\cos\theta_2} \frac{dE}{dx}(out) \right] x \qquad \ldots 4.2$$

where the 'in' and 'out' in brackets refer to the constant values of dE/dx along the inward and outward paths. KE_0 is the energy of the backscattered alpha particles at the surface atoms of the target, while E_1 is the energy of the alpha particle backscattered from the atom at depth x.

Now if one takes the difference between E_1 and kE_0 to be ΔE, i.e.

$$\Delta E = KE_0 - E_1 \qquad \ldots . 4.3$$

Then equation 4.2 can be written as:

$$\Delta E = [S]x \qquad \ldots 4.4$$

where

$$[S] = \left[\frac{K}{\cos\theta_1} \frac{dE}{dx}(in) + \frac{1}{\cos\theta_2} \frac{dE}{dx}(out) \right] \qquad \ldots 4.5$$

[S] is called the energy loss factor that contains the relationship between energy and depth information. It also relates the energy width δE to depth resolution δx: $\delta x = \delta E / [S]$. Therefore, from measuring the energy which can be converted to depth as will be discussed in chapter 5, the backscattered spectrum of counts vs. energy can easily be converted into counts vs. depth.

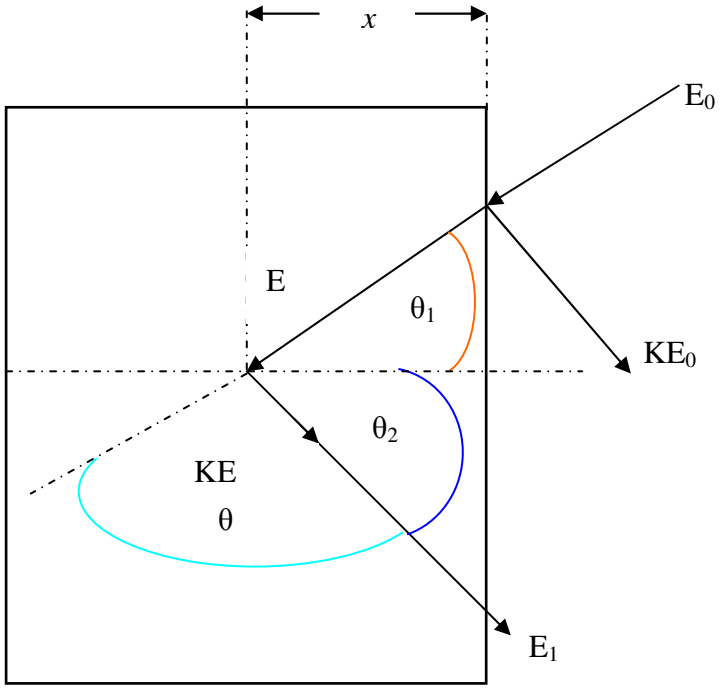

Figure 4-3: A schematic diagram showing the backscattering events in a target consisting of one element. The angles θ_1 and θ_2 are positive regardless of the side on which they lie with respect to the normal of the target.

4.1.5 DIFFERENTIAL CROSS SECTION

Up till now the backscattered α-particle has been discussed without asking: how often does this happen? In order for one to obtain an idea of how frequently this process occurs, the concept of a differential cross section must be introduced.

The probability for a backscattering event to take place is expressed in terms of the differential cross section for scattering, i.e. $d\sigma / d\Omega$ in a given direction into a solid angle $d\Omega$, and is defined as the number of particles scattered into this solid angle $d\Omega$ per number of incident particles per unit area. The differential cross section for the

scattering of a projectile into a solid angle $d\Omega$ centred around an angle θ in the laboratory frame of reference is given as [Chu78][Tes95]:

$$\frac{d\sigma}{d\Omega} = \left(\frac{Z_1 Z_2 e^2}{4E_0} \right)^2 \frac{4(\sqrt{M_2{}^2 - M_1{}^2 \sin^2\theta} + M_2 \cos\theta)^2}{M_2 \sin^4\theta \sqrt{M_2{}^2 - M_1{}^2 \sin^2\theta}} \qquad \ldots 4.6$$

and the total number of detected particles can be written as:

$$A = \sigma \Omega Q N \qquad \ldots 4.7$$

where E_0 is the energy of the projectile before scattering, Z_1 is the atomic number of the projectile with mass M_1, Z_2 is the atomic number of the target with mass M_2, e is the electronic charge, A is the number of backscattered and detected projectiles, Q is the total number of incident projectiles, N is the total number of target atoms per unit area, σ is the differential cross section and Ω is the solid angle of the detector. From equation 4.7 it is clear that when A, σ, Ω and Q are known N can be obtained, thus quantifying the results.

Since the differential cross section is proportional to Z_2^2 and inversely proportional to E_0^2, it means RBS is more sensitive for the detection of elements with higher Z and one could therefore expect more backscattered count/yield if one is working with lower energy compared with higher energies.

4.2 RUTHERFORD BACKSCATTERING SPECTROSCOPY COMBINED WITH CHANNELLING (RBS-C)

RBS-C is a technique that is based on the analyses of the backscattering particles in the channelling direction explained in section 3-5. This is done by perfectly aligning the beam along the crystallographic direction of the sample using a three axis goniometer. Hence, in order to align the beam precisely, the structure of the material of interest needs to be understood. In this section, the structure of SiC is discussed before the RBS-C.

SiC is a binary compound with equal amounts of Si and C atoms. The fundamental structural unit of SiC is a covalently bonded primary co-ordinated elementary tetrahedron, either SiC_4 or CSi_4 [figure 4-4(a)]. These four bonds directed to the neighbours possess an almost pure covalent character, and from the difference in electronegativity between the silicon and the carbon atom, an ionic contribution to the bond of about 12% is estimated.

In a SiC crystal the tetrahedra are arranged in such a way that all atoms lie in parallel planes on the nodes of regular hexagonal networks. The most remarkable characteristic of the crystal structure of SiC is polytypism (which is due to one-dimensional disorder, allowing many structures with different stacking sequences). The difference between various polytypes is the stacking order of elementary tetrahedra [Wes96]. There are two stacking sequences: if the projections of silicon atoms in three successive layers are in different positions A (circles), B (squares) and C (triangles), the cubic structure is formed (figure 4-4(b)); while if the projection of atoms in the third silicon layer coincides with the position A of the first silicon atoms in the first layer (figure 4-4(c)), the hexagonal structure is formed. The SiC crystals appear in a number of modifications that display either hexagonal or trigonal symmetry. They can all be described in the usual hexagonal axis system, with one ***c***-axis perpendicular to three equivalent axes *a*, *b*, and *d* at angles of 120^0 with one another. The axes and the base of the hexagonal unit cell are indicated in figure 4-4(b). Figure 4-4(b) and figure 4-4(c) illustrate that $(11\bar{2}0)$ planes give a correct representation of the SiC structure because all relevant atoms lie in these planes and the right hand figures in figure 4-4 demonstrate such representations for the cubic (zincblend) and hexagonal (wurtzite). The positions of silicon atoms in $(11\bar{2}0)$ planes for most common polytypes of SiC are depicted in figure 4-5. The bold horizontal lines mark the completion of a unit cell on the c-axis. The zinc blend structure requires three steps in the same direction, leading to the stacking sequence ABCABC, known as 3C according to the nomenclature of Ramsdell [Ram47]. A unit cell of the wurtzite lattice is built up by a sequence of one step to the right and one to the left, leading to the stacking sequence of ABAB (figure 4-5(b)), and is called 2H.

All other polytypes can be characterized in this way as shown in figures 4-5(c) and 4-5(d) for 4H and 6H respectively. Figure 4-5(e) portrays the most common modification with a rhombohedral unit cell 15R.

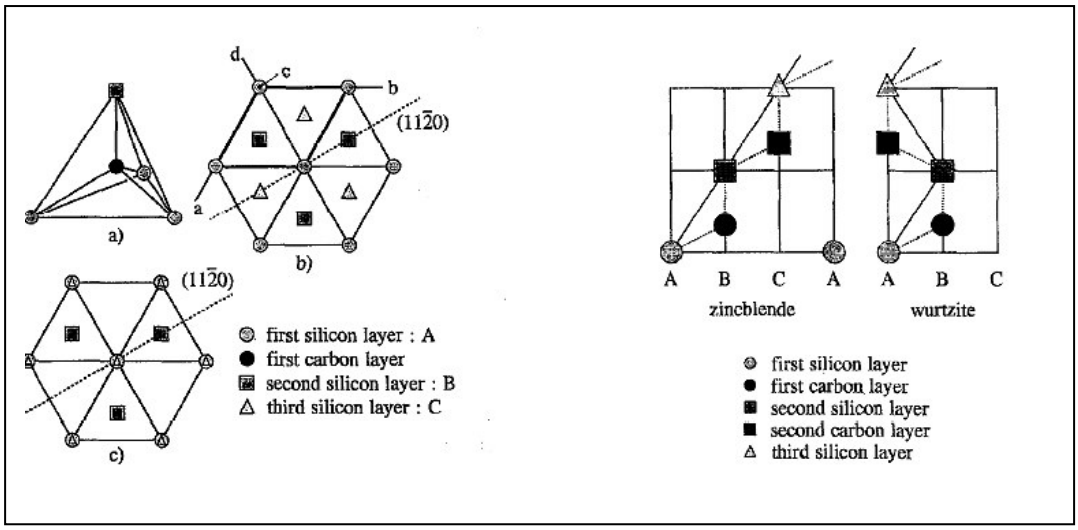

Figure 4-4: Elementary SiC-tetrahedron (a) and projections of different positions of silicon atoms in the zincblende structure; the unlabelled diagrams on the right hand side indicate the position of silicon and carbon atoms in (11$\bar{2}$0) planes of the cubic (zincblende) and hexagonal (wurtzite) structures [Wes96].

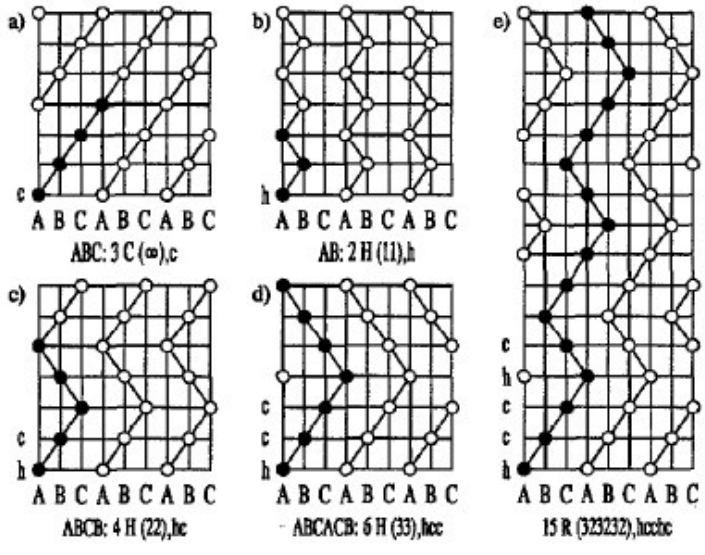

Figure 4-5: Position of silicon atoms in (11$\bar{2}$0) planes of different polytypes [Wes96].

Another form of nomenclature counts the steps necessary to complete one unit cell (the number of steps to the right, then to the left etc. until the unit cell is completed) as

with Zhadanov [Zha45], indicated in figure 4-5 (in brackets). Still other nomenclatures characterize the sequence of layers by cubic (c) or hexagonal (h) environment, as does Jagodzinsky [Jag49]. Different nomenclatures are discussed in [Izh00] [Pag90]. The cubic polytypes are known as β–SiC, and all non-cubic structures (hexagonal and rhombohedra) are called α–SiC. More than 250 polytypes are known to exist.

The RBS-C measurements required a major channel in a crystal, i.e. in 6H-SiC in our case. In the process of finding this channel, the c-axis is taken as the reference. Hence the major channel is searched with reference to the c-axis. In this study, the channel was searched by scanning the sample around a vertical axis perpendicular to the c-axis and around a horizontal axis perpendicular to the c-axis in steps of 0.2^{o}. This scanning was carried out between the Si and C edges to avoid the surface backscattering. This was achieved by setting the backscattering energy window between the Si and C edges using the single channel analyser (SCA) discussed in section 5.5. The yield/counts as a function of these angles on both axes are recorded. The minimum backscattered yields as a function of the angles are then plotted on graph paper. This minimum yield represents the crystallographic planes. The angular scan is then reduced until the directions of planes are determined by plotting the minimum yield as a function of the angles. The crossing point of planes indicates the position of the axis or the channel. After obtaining the channel the energy window is maximized to allow the collection of the full spectrum (in our case the spectrum of SiC with a silver implant).

In this study RBS-C is used to study damage retained in 6H-SiC after implantation and after annealing. The random spectrum is taken 5^{o} off the channel and the target is continuously rotated about the incident c-axis to avoid channelling in the sample. A rough method of estimating an idea of how much damage was present in the sample was devised by comparing the ratio of the aligned spectrum yield/counts of the treated sample to its random spectrum. In this method, if the ratio of the aligned spectrum yield of the treated samples to the random spectrum is equal to 1, it may mean either amorphous or highly disordered or polycrystalline re-growth. The data acquisition of

RBS and RBS-C measurements is described in chapter 5 while results are presented and discussed in chapter 7.

4.3 SCANNING ELECTRON MICROSCOPY (SEM)

A scanning electron microscope (SEM) is a microscope that uses electrons rather than light to form an image of objects on a very fine scale. This kind of microscopy has a long history. The first SEM was built around 1938, with the first commercial instrument being made available around 1965. The electrons are produced in the electron gun by the electron beam source. The function of the electron gun is to provide a stable electron beam of adjustable energy. Older SEMs use tungsten or LaB_6 thermionic emitters while some of the new SEMs are equipped with cold, thermal or Schottky field emission sources. A field emission cathode is usually a wire shaped into a sharp tip (100 nm or less radius) supported by a tungsten hairpin. When the field at the tip reaches a magnitude of about 10V/nm, electrons are emitted. A cathode current density as high as 10^5 A/cm^2 may be obtained from a field emitter as compared with 3 A/cm^2 from a thermionic source [Gol03].

A cold field emitter (CFE) relies purely on the high applied field to cause the emission of electrons. Cold field emitters require an ultrahigh vacuum to ensure that the cathode surface is atomically clean. The tip is flushed clean by heating for a few seconds at about 2500K before the operation. This flushing shortens the lifetime of the emitter. The advantage of the CFE is the virtual probe of 3-5 nm that requires little demagnification to obtain a 1 nm diameter probe. A thermal field emitter (TFE) possesses the same properties as a CFE, but it is operated at elevated temperature. This helps to keep the tip clean, reducing noise and instability even in degraded vacuum conditions. In the Schottky field emitter (SFE) the work function is reduced by a ZrO_2 film deposited on the flattened tip from a small dispenser. An ultrahigh vacuum aids long-term stability, prevents poisoning of the ZrO_2 cathode and maximizes brightness.

The stability of an electron gun is a measure of how constant the electron emission is per unit time. The most stable sources are Schottky field emitters with a beam current stability of about 1%/h.

The electron beam energy spread is the spread in energies of electrons leaving the filament. For a tungsten hairpin gun it is 3 eV, for LaB_6 1.5 eV while it is 0.3-0.7 eV for field emitters. The electron beam is guided into the aperture by magnetic lenses. The aperture determines the current in the final probe of the sample. The probe is scanned across the sample, and the signal produced is detected and amplified before being displayed on the monitor.

Before we discuss this process in detail, we first need to understand the electron material interactions. Figure 4-6 depicts the particles that are produced when the electrons interact with the sample while figure 4-7 illustrates the different depth regimes of the emitted particles. These regimes can overlap for some of the rays; e.g. X-rays also originate from the surface regions. A backscattered electron (e^-) is the result of an elastic collision between an incoming electron and the nucleus of the target atom. The elements with higher atomic numbers produce more backscattered electrons. These electrons usually possess higher energies compared to the energies of the secondary electrons. The detected signal of the former electrons is used for contrast between areas with different chemical compositions, i.e. it is made use of to look at the atomic number contrast and topographical contrast. For example, in the image formed by these electrons, silver will appear brighter than Si and C of SiC because of higher *Z*. Backscattered electrons can also be used to form an electron backscatter diffraction (EBSD) image, which can be utilised to determine the crystallographic structure of the sample [Cha86].

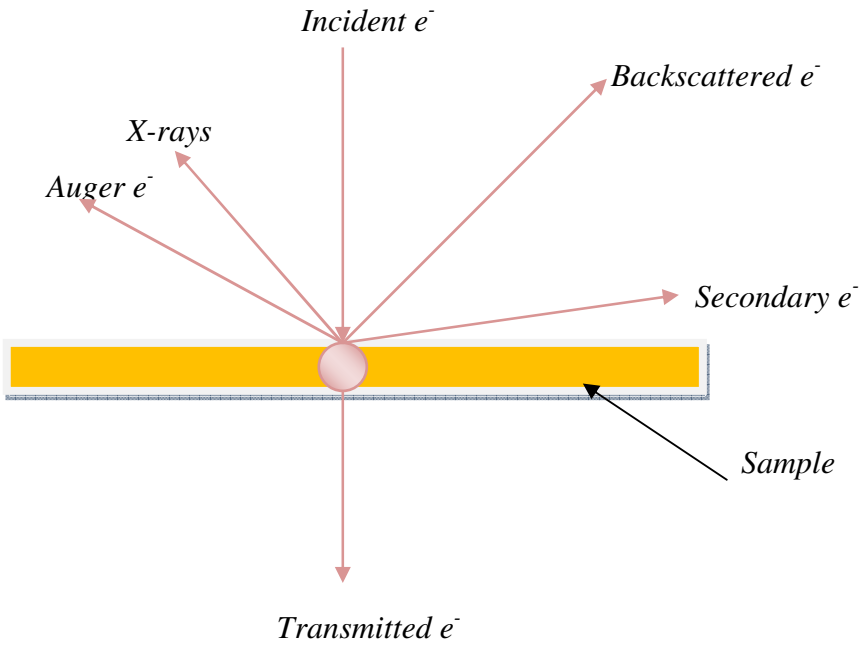

Figure 4-6: A schematic diagram showing what rays are emitted when an energetic electron (e^-) strikes the sample.

Secondary electrons are the results of the inelastic collisions between the incident electrons and the electrons of the target atoms. These electrons possess energy less than 50 eV [Gol03]. Their signal is used to study the surface topography of the sample. These electrons are generated along the incident electrons' trajectory but only those generated a few nano-meters underneath the sample surface are detected – the others are absorbed in the sample owing to their low energy.

Auger electrons are the results of outer shell electrons (higher energy level) filling inner shell holes (lower energy level) created by the excitation primary electron. The excess energy available may be carried away through the emission of low energy electrons (Auger electrons) or the production of X-rays. The signals that result from these Auger electrons can be used for chemical analysis of the sample surface. The X-ray signals can also be utilised for chemical characterization of the samples, i.e. for identifying the type and the concentration of the elements in the sample. The latter technique is called energy dispersive x-rays spectroscopy (EDS).

The volume at which all the discussed interactions occur in the sample depends on the following three factors: Atomic number of the material that is being analysed since a higher atomic number sample absorbs or stops more electrons and causes a smaller interaction volume. Electron energy: higher energy electrons penetrate further into the sample and generate a larger interaction volume. The angle of incidence for the electron beam: the greater the angle (further from normal), the smaller the interaction volume. By detecting the necessary signals, SEM is able to provide information on the following:

(i) Topography, which identifies the features of the surface of an object or sample.

(ii) Morphology, which furnishes information on the shape and the size of the particles making up the sample.

(iii) Composition, in other words the elements and compounds that the sample is composed of and the relative amounts of them (this is possible in some SEMs).

(iv) Crystallographic information, which shows how the atoms are arranged in the sample.

In this study, a Zeiss Ultra 55 field emission scanning electron microscope which uses SFE was used. This machine employs a field emission electron gun. The Zeiss Ultra 55 is equipped with SE (secondary electron) detectors, BE (backscattered electron) detectors and an in-lens SE detector. The last mentioned is a detector which is highly surface sensitive; its efficiency improves as the acceleration voltage drops lower. For most of our studies the in-lens SE detector was used to study the surface before and after annealing. The results are discussed in chapter 7.

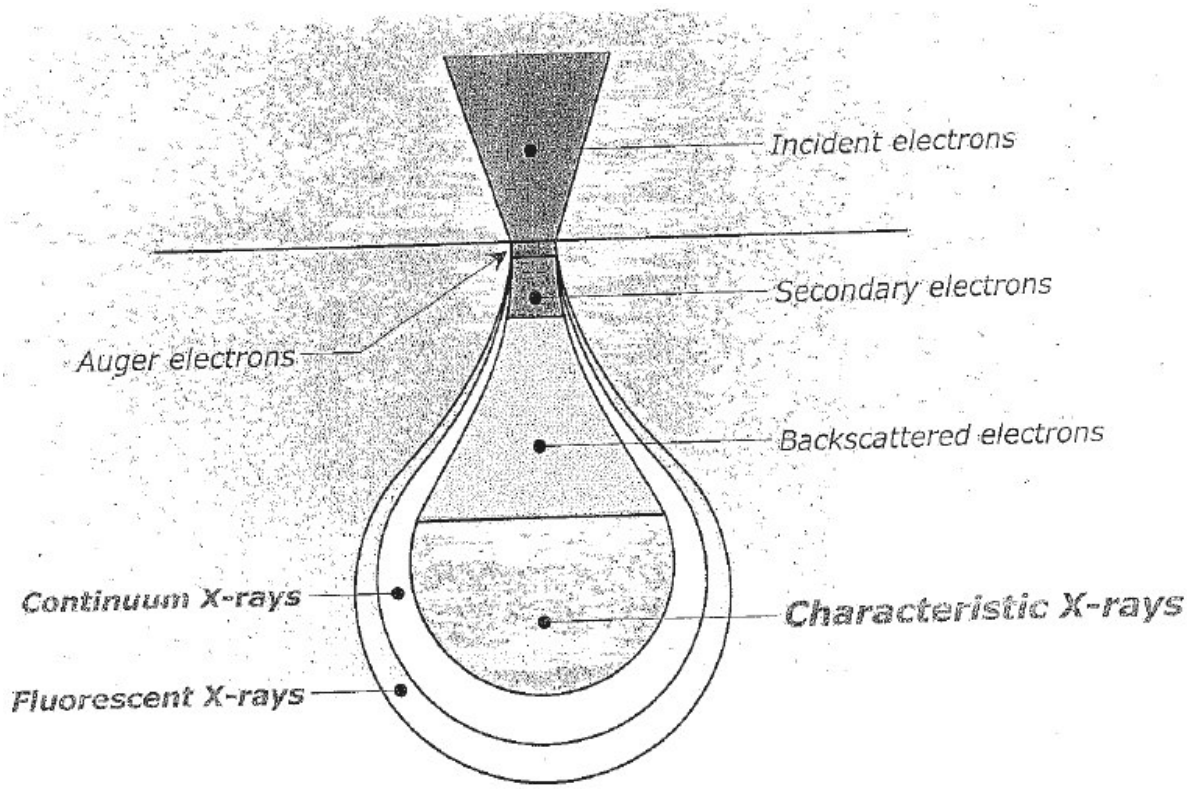

Figure 4-7: A schematic diagram showing that the particles emitted during electron-sample interaction are emitted at different depths [wwwi].

4.4 REFERENCES

[Cha86] S.K. Chapman, Working with an Electron Microscope, Lodge-marks Press (1986).

[Chu78] W. K. Chu, J. W. Mayer and M. A. Nicolet, Backscattering Spectrometry, Academic Press, New York (1978).

[Gär05] K. Gärtner, Nucl. Instr. and Meth. **B227** (2005) 522.

[Gär97] K. Gärtner, K. Hehl, G. Schlotzhauer, Nucl. Instr. and Meth. **B4** (1984) 55 und 63; K. Gärtner Nucl. Instr. and Meth. **B132** (1997) 147.

[Gol03] J. Goldstein, D. Newbury, D. Joy, C. Lyman, P. Echlin, E. Lifshin, L. Sawyer and J. Michael, Scanning Electron Microscopy and X-Ray Microanalysis, 3rd edition, Springer, USA (2003).

[Gra31] R. J. van de Graaff, Phys. Rev. **38** (1931) 1919.

[Izh00] V. A. Izhevskyi, L. A. Genova, J. C. Bressiani, A. H. A. Bressiani, Cerâmica vol.46 n.297, São Paulo Jan./Feb./Mar. 2000.

[Jag49] H. Jagodzinski, Acta Crystallog., **2** (1949) 201-207.

[Pag90] T. F. Page, The Physics and Chemistry of Carbides, Nitrides and Borides. Edited by R. Freer, Kluwer Acad. Publishers, Netherlands, (1990) 197.

[Ram47] R. S. Ramsdell, Am. Min., **32** (1947) 64.

[Tes95] J. R. Tesmer and M. Nastasi, Handbook of Modern Ion Beam Materials Analysis, MRS., Pittsburgh (1995).

[Wes96] W. Wesch, Nucl. Instr. and Meth. **B116** (1996) 305.

[www1] http://www.jeol.com,12, November, 2010.

[Zha45] G. R. Zhadanov, Compte Rende Acad. Sci. URSS, **48** (1945) 39.